**Proceedings of the ASME 2013 International Design Engineering Technical Conferences &
Computers and Information in Engineering Conference
IDETC/CIE 2013
August 4-7, 2013, Portland, USA**

# DETC2013/12909

# EXPERIMENTAL IDENTIFICATION OF THE COMPLEX DYNAMICS OF A STRONGLY NONLINEAR SPACECRAFT STRUCTURE

**J.P. Noël,[*] L. Renson, and G. Kerschen**
Space Structures and Systems Laboratory
Department of Aerospace and Mechanical Engineering
University of Liège
Liège, Belgium

## ABSTRACT

*The present paper addresses the identification of a real-life spacecraft structure possessing an impact-type nonlinear component. The complete identification procedure, i.e. from non-linearity detection to parameter estimation, is carried out using experimental data collected during a typical spacecraft qualification test campaign. The complementary use of several techniques reveals particularly interesting and complex phenomena such as nonlinear jumps, nonlinear modal interactions, internal force relaxation and chattering during impacts.*

## INTRODUCTION

Nonlinear system identification is known to be a challenging task in view of the complexity and variety of nonlinear dynamical phenomena. Significant progress has been performed in the last twenty years or so [1] and, to date, multi-degree-of-freedom lumped parameter systems and simple continuous structures with localised nonlinearities are within reach. However, the identification of large-scale engineering structures with multiple, and possible strongly, nonlinear components remains a distinct challenge and concentrates current research efforts. In this context, the present paper addresses the identification of the SmallSat spacecraft, a strongly nonlinear real-life structure developed by EADS-Astrium. Nonlinearity is caused by mul-

tiple mechanical stops limiting the motion of an inertia wheel mounted on an elastomeric interface.

The complete identification procedure, *i.e.* from nonlinearity detection to parameter estimation, is carried out using experimental data collected during a typical spacecraft qualification test campaign. Several techniques, which include the mere visual inspection of time series, time-frequency analysis and the restoring force surface method [2] are utilised to bring complementary perspectives to the dynamics. Specifically, the spacecraft is shown to exhibit particularly interesting and complex phenomena such as nonlinear jumps, nonlinear modal interactions, internal force relaxation and chattering during impacts. In particular, nonlinear modal interactions are revealed using the wavelet transform and compared with numerical predictions obtained using continuation algorithms applied to a finite element model of the structure.

## THE SMALLSAT SPACECRAFT

The SmallSat structure was conceived by EADS-Astrium as a low-cost platform for small satellites in low earth orbits [3]. It is a monocoque tube structure which is 1.2 *m* long and 1 *m* large. It incorporates eight flat faces for equipment mounting purposes, creating an octagon shape, as shown in Figure 1. The interface between the spacecraft and the launch vehicle is achieved through four aluminium brackets located around

---

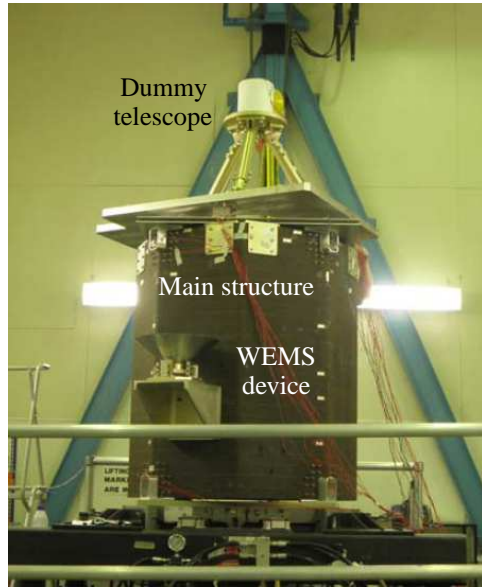[*]Address all correspondence to this author, email: jp.noel@ulg.ac.be.

**FIGURE 1**: SMALLSAT SPACECRAFT.

cut-outs at the base of the structure. The total mass including the interface brackets is around 64 *kg*.

The spacecraft structure supports a dummy telescope composed of two stages of base-plates and struts supporting various concentrated masses; its mass is around 140 *kg*. Besides, as depicted in Figure 2 (a), a support bracket connects to one of the eight walls the so-called Wheel Elastomer Mounting System

(WEMS) device which is loaded with an 8 *kg* dummy inertia wheel. The WEMS device is a mechanical filter which mitigates disturbances coming from the inertia wheel through the presence of a soft elastomeric interface between its mobile part, *i.e.* the inertia wheel and a supporting metallic cross, and its fixed part, *i.e.* the bracket and by extension the spacecraft. Moreover, eight mechanical stops limit the axial and lateral motions of the WEMS mobile part during launch, which gives rise to strongly nonlinear dynamical phenomena. A thin layer of elastomer placed onto the mechanical stops is however utilised to prevent metal-metal impacts. Figure 2 (b) presents a simplified though relevant modelling of the WEMS device where the inertia wheel, owing to its important rigidity, is seen as a point mass. The four nonlinear connections (NCs) between the WEMS mobile and fixed parts are labelled NC 1 – 4. Each NC possesses a trilinear spring in the axial direction (elastomer in traction plus two stops), a bilinear spring in the radial direction (elastomer in shear plus one stop), and a linear spring in the third direction (elastomer in shear). In Figure 2 (b), linear and nonlinear springs are denoted by squares and circles, respectively.

During the qualification test campaign, swept-sine base excitations were applied to the spacecraft for different amplitude levels and directions. Two specific data sets are studied in the present work, measured under 0.6 and 1 *g* axial (Z) loadings and for positive sweep rates of 2 and 4 octaves per minute, respectively. They are further restricted to the analysis of a single local WEMS mode of vibration between 5 and 15 *Hz*. The corresponding modal shape is a swing motion of the WEMS mobile part around Y axis which causes axial impacts in the NC 1 and NC 2.
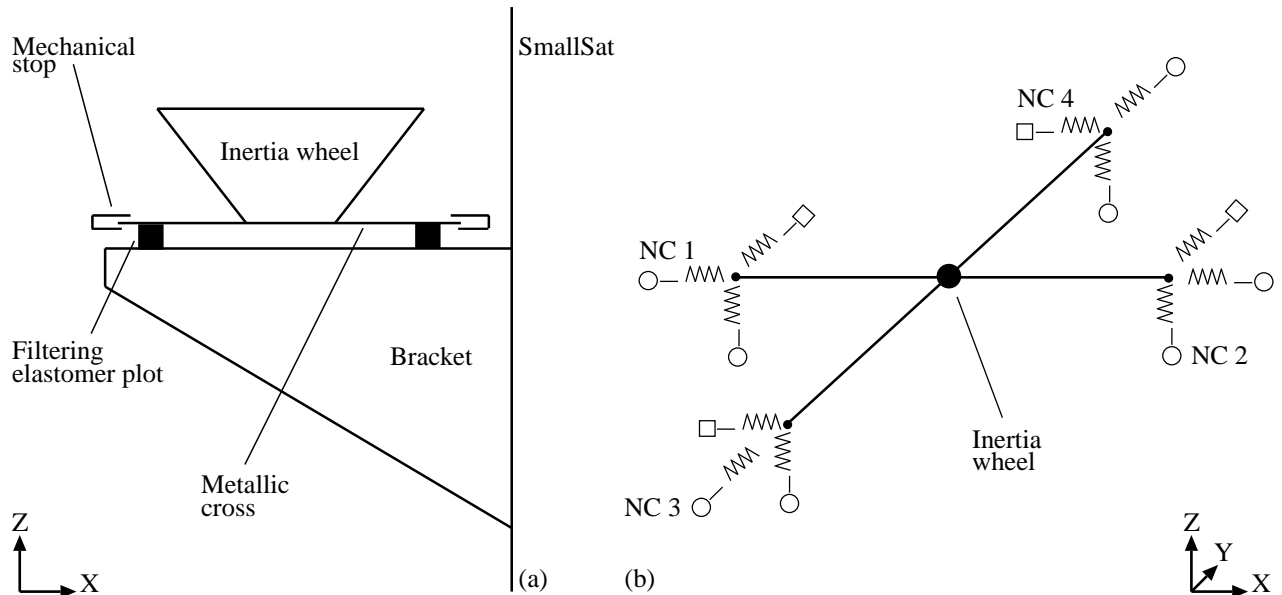


**FIGURE 2**: WEMS DEVICE. (a) DETAILED DESCRIPTION; (b) SIMPLIFIED MODELLING OF THE WEMS MOBILE PART.

## DETECTION OF NONLINEAR BEHAVIOUR

Nonlinearity detection basically boils down to seeking departures from linear theory predictions. In this regard, stepped- and swept-sine excitations are particularly convenient because, if linear, the structure is known to generate a pure sine wave in output. Harmonic distortions can sometimes be such that a mere visual inspection of the raw time series is sufficient to reveal nonlinear behaviour. To this end, the axial relative displacement across the NC 1 measured at 0.6 $g$ and 1 $g$ is plotted in Figures 3 (a – b), respectively. Note that the measured accelerations were integrated using the trapezium rule and then high-pass filtered to obtain displacement signals. For confidentiality reasons, relative displacements are adimensionalised throughout the paper.

### Envelope-based detection

A first observation is the absence of proportionality between the time responses in Figures 3 (a – b). This is particularly visible for negative displacements where the maximum amplitude reached at 0.6 $g$ and 1 $g$ is almost unchanged. This violates the principle of superposition, a cornerstone of the linear theory. One further remarks that the resonance peak is no longer smooth in Figure 3 (b) but exhibits a nonlinear jump phenomenon, *i.e.* a sudden transition from large to small amplitudes of vibration, which confirms the activation of nonlinearity at 1 $g$.

### Close-up-based detection

At 0.6 $g$, the resonance peak shows no evidence of nonlinearity. However, a close-up analysis of the response in 8.1 – 8.4 $Hz$, as achieved in Figure 3 (c), reveals the presence of harmonics in the time series. A similar inspection at 1 $g$ in 8.4 – 8.7 $Hz$ depicted in Figure 3 (d) shows much more significant harmonics and a limitation of the amplitude of motion in negative displacement resulting in the asymmetry of the response.

### Phase-plane diagram

An under-utilised yet useful means of revealing harmonic distortions is a phase-plane diagram, which follows an ellipse in the case of a pure sine wave. The relative displacements of Figures 3 (c – d) are consequently plotted against the corresponding relative velocities to generate phase-plane trajectories in Figures 3 (e – f), respectively. The existence of harmonics at 0.6 $g$ is now obvious, and the activation of a strongly nonlinear regime of vibration is confirmed at 1 $g$.

### Nonlinear jump phenomenon

The nonlinear jump phenomenon observed in Figure 3 (b) is worth being studied in more detail. It is an intrinsic manifestation of nonlinearity which has no linear counterpart. It stems from the existence of multiple stable solutions between which the nonlinear system can suddenly switch for small variations of the forcing frequency. A meaningful representation of the jump is achieved in the phase plane in Figure 4 (a) where the excitation frequency parametrises the curve as a colour map. The sudden transition from a nonlinear to a linear regime of vibration can precisely be located at 9.4 $Hz$. This transition is even better perceived in a phase-plane plot of the internal force across the NC 1, as in Figure 4 (b). In this three-dimensional representation, nonlinear oscillations before the jump correspond to the outer trajectories and are clearly seen to be associated with impacts in the force pattern.

## NONLINEARITY CHARACTERISATION

Beyond detection, useful insight into the nonlinearity can be gained through visual inspection. For instance, the presence of shocks in Figure 3 (d), which are already visible in Figure 3 (c), is the symptom of a non-smooth nonlinearity. Moreover, because they only appear for negative relative displacements, the clearance in the – Z direction is found to be smaller than in the + Z direction. This asymmetry can be explained by the prestress applied to the elastomer plots by gravity. The amplitude-limiting effect of the NC 1 stop, observed within the oscillations in Figure 3 (d), finally yields a direct estimation of the – Z clearance around 1.

### Histogram

A particularly meaningful representation of the measured time series for clearance estimation is a histogram. This is achieved in Figures 5 (a – b) for the relative displacements of Figures 3 (a – b), respectively. The accumulation of samples in the left-hand tails of the typical double-peak-shaped distributions of sine waves confirms the asymmetry of the WEMS device and the location of the NC 1 negative clearance around 1.

### Restoring force surface method

The restoring force surface (RFS) method relies on Newton's second law of motion, written for a single-degree-of-freedom (SDOF) system as
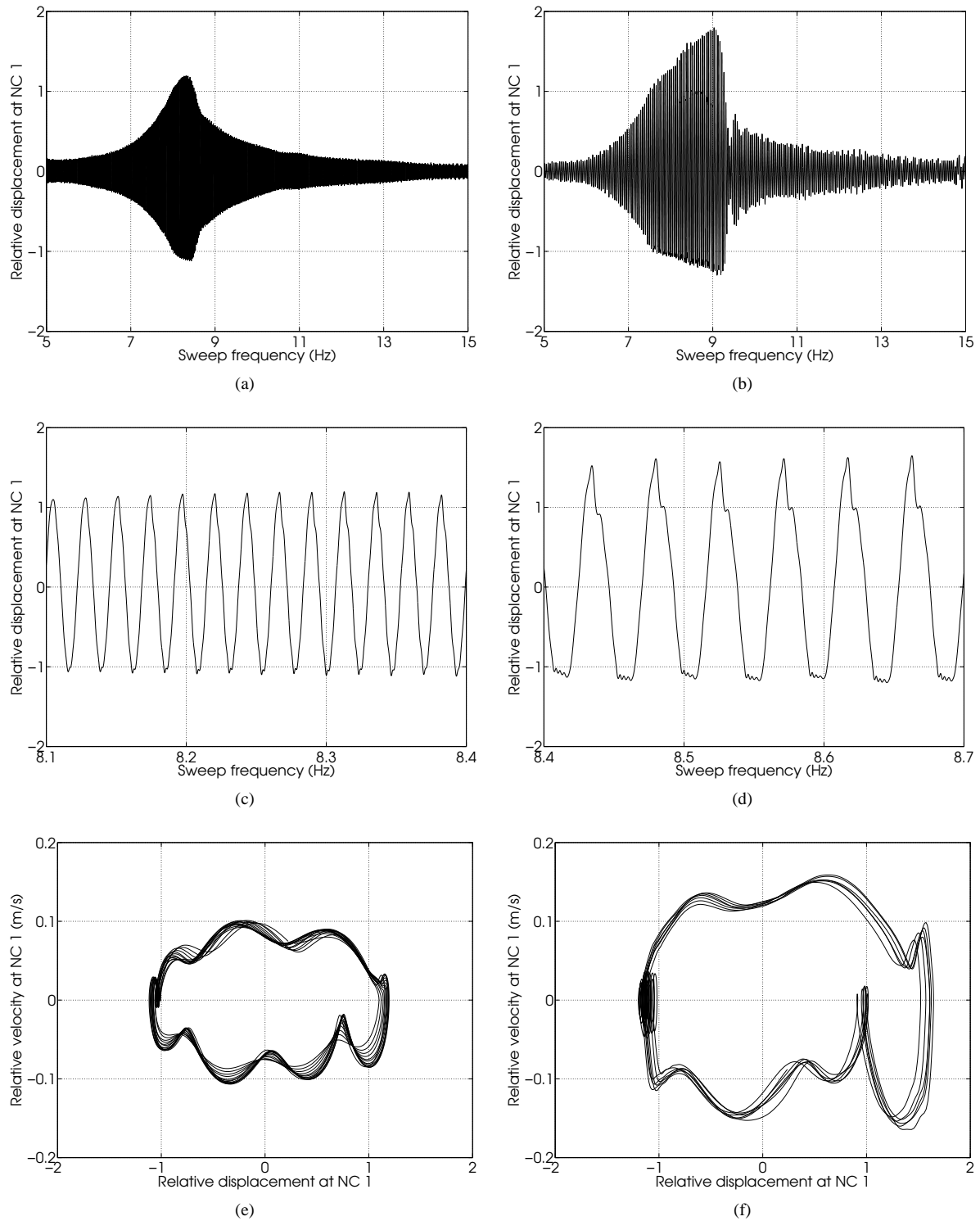
$$m\ddot{x} + f(x, \dot{x}) = p \qquad (1)$$

**FIGURE 3**: NONLINEARITY DETECTION AT 0.6 g (LEFT COLUMN) AND 1 g (RIGHT COLUMN). (a – b) ENVELOPE-BASED ANALYSIS; (c – d) CLOSE-UP OF THE DISPLACEMENT SIGNAL; (e – f) PHASE-PLANE DIAGRAM.
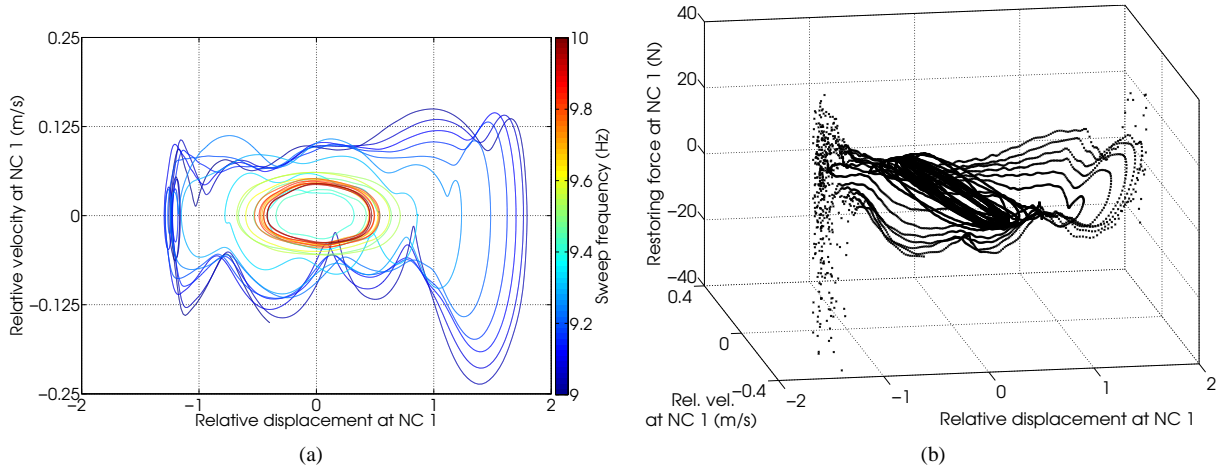
(a)



(b)

**FIGURE 4**: NONLINEAR JUMP PHENOMENON. (a) PHASE PLANE; (b) INTERNAL FORCE.

where $m$ is the mass, $\ddot{x}$ the acceleration and $p$ the external force and where $f$ encompasses all the restoring forces in the system, being of elastic or dissipative nature. This equation recast into

$$f(x, \dot{x}) = p - m\ddot{x} \qquad (2)$$

gives a direct access to a nonparametric estimation of the restoring force surface defined by the triplets $(x, \dot{x}, f(x, \dot{x}))$. Applied to more complex systems, the method only yields qualitative information but can still be exploited for visualising nonlinear effects. The NC 1 force-displacement curves at 0.6 $g$ and 1 $g$ are shown in Figures 5 (c – d), respectively. They reaffirm the discontinuous nature of the nonlinearities in the system, the asymmetry in the WEMS behaviour and the location of the − Z clearance around 1. In comparison with other techniques, the restoring force curve at 1 $g$ also highlights the activation of the + Z stop, beyond a relative displacement of about 1.5. A comprehensive estimation of the NC 1 and NC 2 clearances will be realised in the next section.

**Time-frequency analysis**

The wavelet transform is arguably one of the most versatile tools for interpreting harmonic components generated by nonlinear systems. The wavelet amplitudes of the relative displacements of Figures 3 (a – b) are displayed in a logarithmic scale in Figures 5 (e – f), respectively. At 0.6 $g$, the presence of several harmonics around 8.5 $Hz$ is an additional confirmation of the presence of impacts in the system. At 1 $g$ in Figure 5 (f), the mechanical stops are reached over a wider sweep window. Impacts are also found to be stronger as confirmed by the relative importance of harmonics in the response. One finally notices that the

jump in Figure 3 (b) closely coincides with the disappearance of wideband frequency components in Figure 5 (f) and that electrical noise pollutes both wavelets through a frequency line around 50 $Hz$.
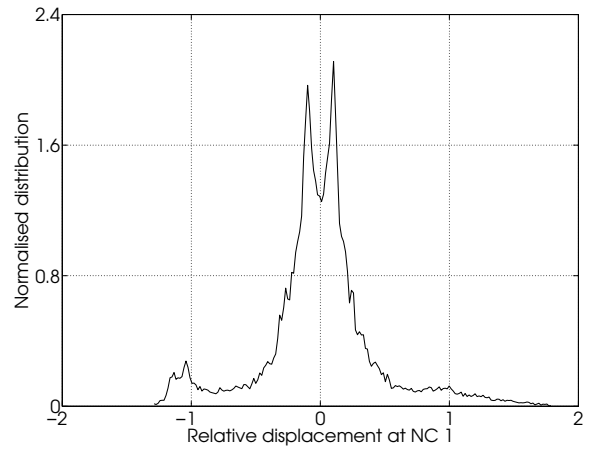
**Nonlinear modal interaction**

The jump phenomenon studied in Figures 4 (a – b) was a first intrinsic manifestation of nonlinearity addressed in the paper. The wavelet transform can reveal another inherently nonlinear phenomenon that has no counterpart in linear theory, namely nonlinear modal interaction. To this end, Figure 6 (a) depicts, in linear scale, the wavelet amplitude of the NC 4 X-displacement over 5 − 35 $Hz$. Higher harmonic components are found to be of comparable amplitude to the fundamental frequency driven by the excitation. In particular, typical 2:1 and 3:2 internal resonances, *i.e.* modal interactions between two nonlinear modes, are observed. One notes that the generation of even harmonics is characteristic of asymmetrical systems. A third harmonics is also visible in Figure 6 (a) but however does not underlie modal interaction because no target mode is present in the adequate frequency band.

Such interactions between nonlinear modes that are not closely-spaced in frequency can be reliably predicted using numerical continuation algorithms [4]. In brief, as a nonlinear mode of vibration is defined as a periodic motion in the undamped case [5], such algorithms seek periodic solutions of the equations of motion for increasing energy levels and track the evolution their frequency. This results in a so-called frequency-energy plot (FEP), computed for each nonlinear mode. A finite
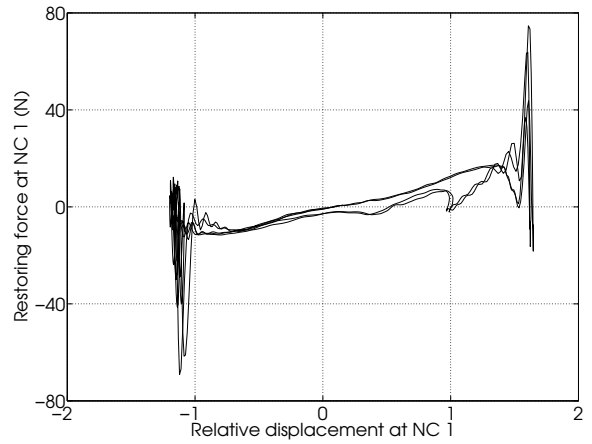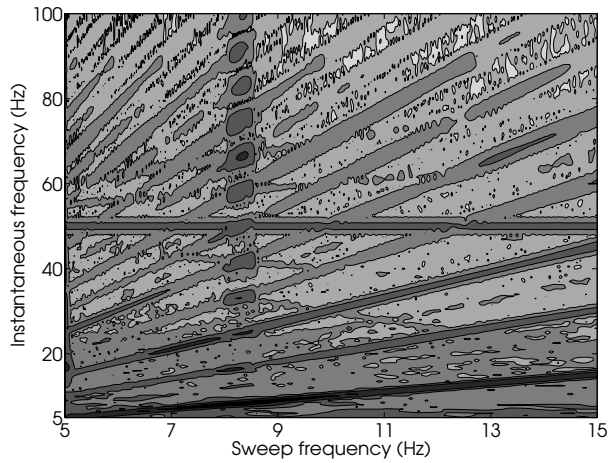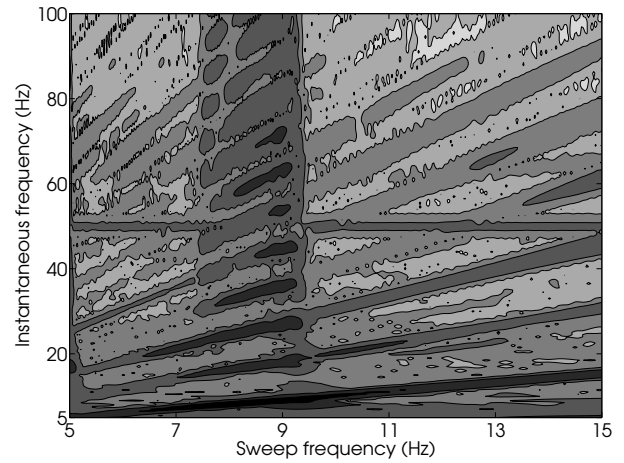
5
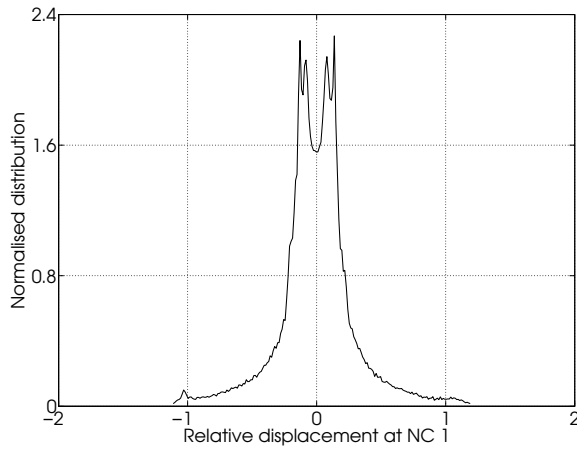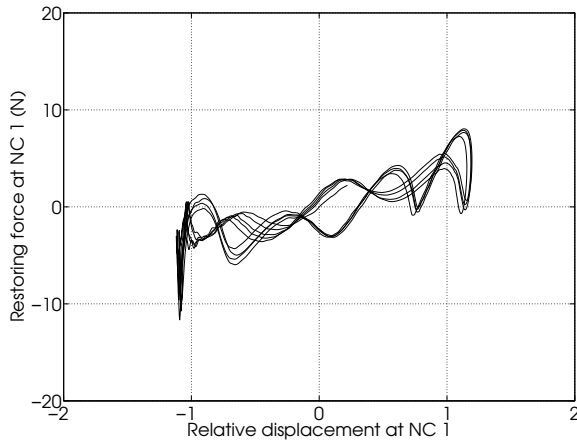
**FIGURE 5**: NONLINEARITY CHARACTERISATION AT 0.6 g (LEFT COLUMN) AND 1 g (RIGHT COLUMN). (a – b) HISTOGRAM; (c – d) RFS METHOD; (e – f) WAVELET TRANSFORM AMPLITUDE.
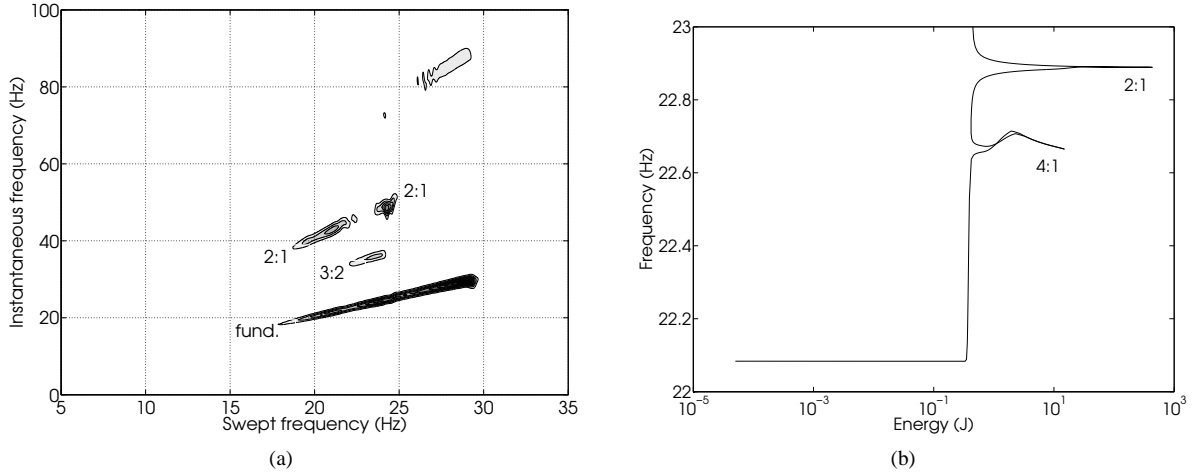
6

(a)

(b)

**FIGURE 6**: NONLINEAR MODAL INTERACTION. (a) EXPERIMENTAL OBSERVATION; (b) NUMERICAL PREDICTION.

element model of the SmallSat was developed [6] and is used in the present study to compute the FEP of the mode located around 22 $Hz$ in Figure 6 (a) which is found to trigger a 2:1 interaction. The calculated diagram is proposed in Figure 6 (b) where the appearance of "tongues" signals the presence of modal interactions and thus confirms the experimental observation. Furthermore, the numerical continuation predicts the possibility of a 4:1 internal resonance, also realised in practice but not displayed herein for the sake of brevity.

## RFS-BASED PARAMETER ESTIMATION

Parameter estimation is the last step towards the establishment of a nonlinear model with good predictive capabilities. This is the most difficult step in the identification process but also the one that conveys the most valuable information about the system under test, namely nonlinear stiffness and/or damping coefficients. A literature survey reveals that the RFS method is the only approach compatible with unmeasured base-sine excitations for parameter estimation. However, its domain of applicability is generally limited to reduced-scale structures since it requires a rigorous writing of Newton's law of dynamics. Thus, system complexity reduction is usually considered, as for instance in [7], where Worden *et al.* studied an automotive shock absorber system that was constrained to move in only one direction to justify a SDOF assumption.

By asserting that the WEMS mobile part, *i.e.* the inertia wheel and its metallic cross-shaped support, behaves as a rigid body, its dynamics can similarly be simplified in order to make it

tractable analytically. Hence we can write

$$m \frac{\ddot{z}_1 + \ddot{z}_2}{2} + f_{NC1}(z_1, \dot{z}_1) + f_{NC2}(z_2, \dot{z}_2) = 0 \qquad (3)$$

where $m$ is its mass evaluated at 8.75 $kg$, $z_i$ the Z-displacement measured at the NC $i$, $f_{NCi}$ the associated nonlinear restoring force including stiffness and damping terms and where an overdot denotes a derivative with respect to the time variable $t$. Contributions related to NC 3 and NC 4 have been neglected in Equation (3) because they involve considerably lower displacement and velocity. It is worth pointing out that rigidity imposes geometrical constraints onto the possible motion of the WEMS. If we denote by $\vec{v}_{12}$ and $\vec{v}_{34}$ the vectors joining opposite NCs, we have

$$\begin{cases} d(v_{12})/dt = d(v_{34})/dt = 0 \\ \vec{v}_{12} \cdot \vec{v}_{34} = 0 \\ \vec{v}_{12}/2 = \vec{v}_{34}/2 \end{cases} \qquad (4)$$

where the third relationship is vectorial and should be understood as an element-by-element mean. Considering the supporting metallic cross in Figure 2 (b), these constraints express the invariability of the length of its two arms, their orthogonality and their common midpoints, respectively. Beyond this geometrical interpretation, they provide a means of assessing the accuracy loss one is willing to pay in exchange for complexity reduction. For this purpose, Figure 7 represents the deviations from rigidity (in %) observed as the excitation frequency increases at 1 $g$ level. Note that 0.6 $g$ results are now skipped in favour of the

more interesting 1 $g$ data set for the sake of conciseness. In general, the six scalar constraints are very well satisfied and so guarantee the quality of our subsequent parameter estimation results. Orthogonality is even found to be exactly verified, as intuitively guessed. The largest errors occur in the X direction, being however limited to 5 % at resonance. This confirms that the WEMS motion in the $5-15\ Hz$ band is mainly a swing oscillation around Y axis entailing impacts onto the NC 1 and NC 2 stops.
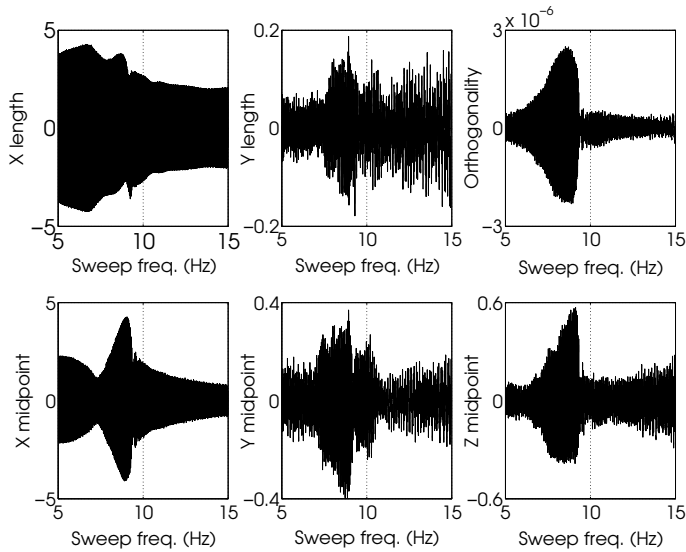


**FIGURE 7**: VERIFICATION OF THE GEOMETRICAL CONDITIONS OF RIGIDITY AT 1 $g$ (IN %).

Figures 8 (a – b) show the stiffness curves measured at the NC 1 and NC 2, respectively, and constructed using Equation (3) in the 8.5 to 9 $Hz$ band to focus on nonlinear data. A first observation is the presence of a quadratic contribution in Figure 8 (a) which is attributed to gravity and is in line with the WEMS asymmetry pointed out several times above (see Figure 5). This term originates from an initial displacement of the system from its gravity-free equilibrium position [8]. Because the bracket hardly bends at the NC 2 and is thus locally close to this latter position, there appears no gravity-induced stiffness term in Figure 8 (b).

Curve-fitting results are reported in Table 1 where stiffness coefficients and clearances are adimensionalised values. One first notices that the calculated stiffnesses of the elastomer plots are in agreement with the reference value of 150 obtained by EADS-Astrium through static deflection tests. Estimates of the nonlinear coefficients match equally well their static reference of

1980 and reveal that impacts are comparatively softer for positive displacements. Each fitted term is given together with a significance factor (SF) in Table 1, given between parentheses and computed as the ratio (in %) between the root-mean-squared values of the considered term and the sum of all model terms. The main conclusion this indicator brings is the low but not negligible importance of the introduced quandratic term. It also shows that the very low number of impacts on the + Z stop in Figure 8 (b) reduces the significance of the corresponding model term. The SF is finally worth being interpreted as an uncertainty measure since the smaller the SF a coefficient has, the more likely its estimation is prone to the noise influence and to modelling errors.

**Internal force relaxation and chattering**

One finally aims at analysing two particularly interesting dynamical phenomena related to the stiffness curves represented in Figures 8 (a – b). In fact, they were constructed as cross sections of the corresponding force surfaces, calculated by means of Equation (3) given the triplets $(z_1, \dot{z}_1, f_{NC1})$ and $(z_2, \dot{z}_2, f_{NC2})$. The surface obtained for the NC 1 is shown in Figure 8 (c) and reveals an asymmetry with respect to the zero-velocity axis. In particular, for negative displacements, the presence of impacts seems to die out as velocity goes from negative to positive values. This suggests a viscoelastic behaviour of the elastomer components in the system, namely internal force relaxation. The phenomenon is better highlighted in Figures 8 (d – e) where the relative displacement and the internal force corresponding to Figure 8 (c) are depicted versus sweep frequency. The analysis of the two graphs clearly demonstrates the decrease of the internal force at constant negative relative displacement. This proves that a reliable estimation of the stiffness properties in the system should be achieved prior to the initiation of stress relaxation. Specifically, cross sections of the restoring force surfaces for velocities lower than -0.07 $m/s$ were considered to plot Figures 8 (a – b).

Besides, it can be estimated that a single relaxation phase lasts 0.025 $s$, which can appear to be extremely fast but may result from the high speed of loading (typically 0.15 $m/s$ and acceleration of about 100 $m/s^2$), the prestress in the elastomer plots and the limited thickness of the elastomer layer hit during impacts. Prestress combined with speed of loading could also explain why relaxation is not manifest for positive relative velocities.

It is also interesting to note that the displacement is not rigorously constant within the relaxation regions but exhibits rapid bounces whose frequency is evaluated at 120 $Hz$ (see Figure 8 (d)). They are interpreted as a contact chattering phenomenon [9] triggered by the conflict between prestress and
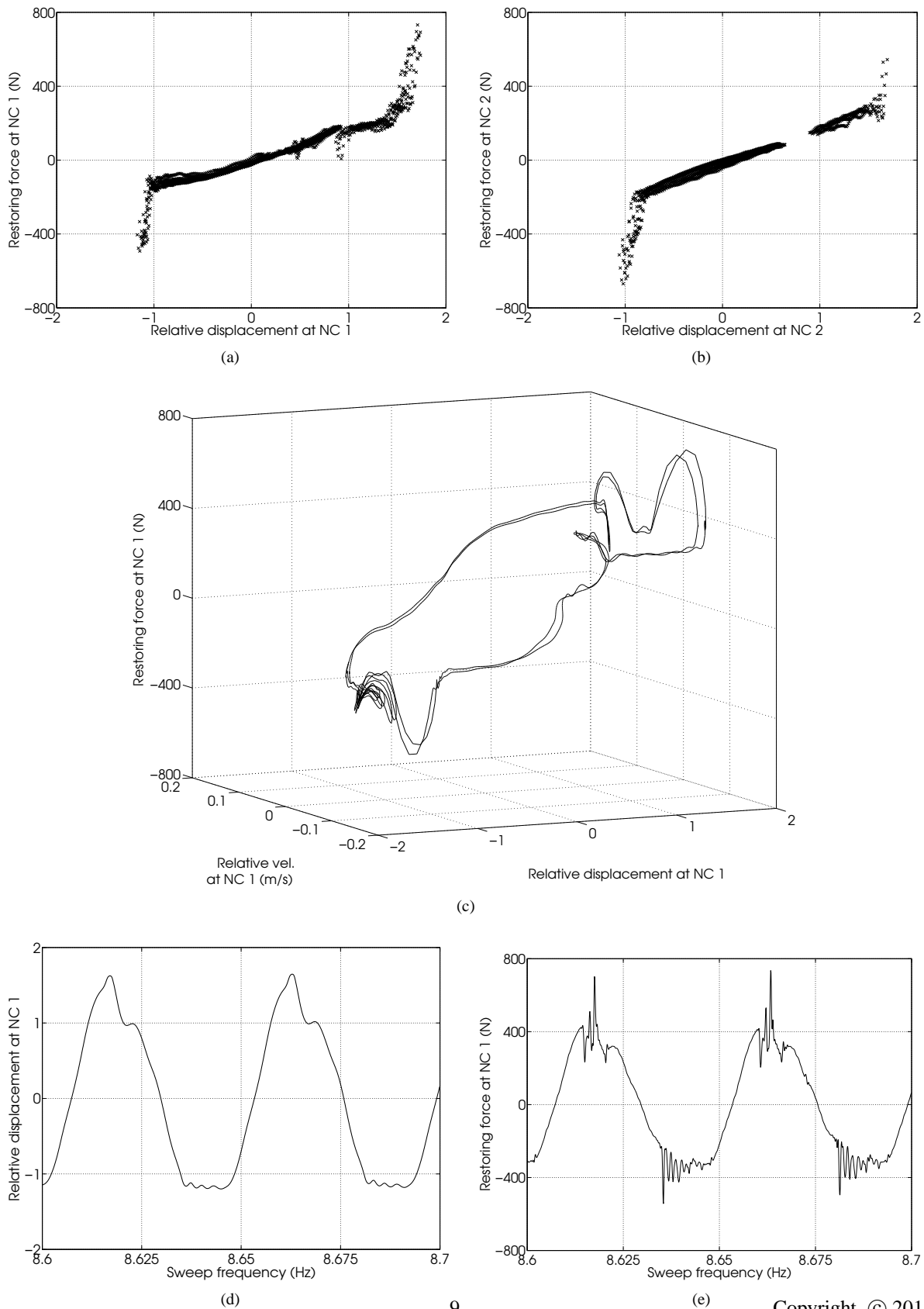
(a)

(b)

(c)

(d)

9

(e)

**FIGURE 8**: WEMS RESTORING FORCES AND EVIDENCE OF INTERNAL FORCE RELAXATION AND CHATTERING. NON-LINEAR STIFFNESS FORCES AT THE (a) NC 1 AND (b) NC 2; (c) COMPLETE RESTORING FORCE SURFACE AT THE NC 1 AND CORRESPONDING (d) RELATIVE DISPLACEMENT AND (e) RESTORING FORCE VERSUS SWEEP FREQUENCY.

**TABLE 1**: STIFFNESS COEFFICIENTS, CLEARANCES AND SIGNIFICANCE FACTORS AT THE NC 1 AND NC 2.

|  | NC 1 | NC 2 |
|---|---|---|
| Elastomer stiffness | 155 (80.0) | 184 (82.5) |
| Quadratic stiffness | 11,847 (5.3) | — |
| Clearance – Z | 1 | 0.84 |
| Stop – Z stiffness | 2,453 (21.5) | 2,257 (34.6) |
| Clearance + Z | 1.55 | 1.62 |
| Stop + Z stiffness | 1,874 (22.5) | 1,907 (4.3) |

restoring forces. Chattering explains why relaxation occurs through oscillations in Figure 8 (e) and not as a monotonic decrease. In the simple Maxwell model for viscoelasticity, the stress is found to decrease exponentially with time at constant strain. The envelope of oscillation in the relaxation regions in the same figure tends towards confirming this prediction.

## CONCLUSIONS

The objective of this paper was to address the identification of a real-life strongly nonlinear space structure, the Small-Sat spacecraft developed by EADS-Astrium. For this purpose, experimental data collected during a typical spacecraft qualification test campaign were exploited. The complete identification procedure, encompassing namely detection, characterisation and parameter estimation, was carried out using several techniques, *e.g.* the mere visual inspection of time series, time-frequency analysis and the restoring force surface method. They allowed to gain very useful insight into the dynamics, including the successful estimation of the clearances and nonlinear stiffness parameters of the system. Finally, the spacecraft was shown to exhibit particularly interesting and complex phenomena in practice, such as nonlinear jumps, nonlinear modal interactions, internal force relaxation and chattering during impacts. In particular, nonlinear modal interactions were revealed using the wavelet transform and compared with numerical predictions obtained using continuation algorithms applied to a finite element model of the structure.

## ACKNOWLEDGEMENTS

## REFERENCES

[1] Kerschen, G., Worden, K., Vakakis, A. F., and Golinval, J., 2006. "Past, present and future of nonlinear system identification in structural dynamics". *Mechanical Systems and Signal Processing,* **20**, pp. 505–592.

[2] Kerschen, G., Golinval, J., and Worden, K., 2001. "Theoretical and experimental identification of a non-linear beam". *Journal of Sound and Vibration,* **244(4)**, pp. 597–613.

[3] Russell, A. G., 2000. "Thick skin, faceted, CFRP, monocoque tube structure for smallsats". In the Proceedings of the European Conference on Spacecraft Structures, Materials and Mechanical Testing.

[4] Peeters, M., Vigiué, R., Sérandour, G., Kerschen, G., and Golinval, J., 2009. "Nonlinear normal modes, Part II: Toward a practical computation using numerical continuation techniques". *Mechanical Systems and Signal Processing,* **23**, pp. 195–216.

[5] Rosenberg, R. M., 1966. "On nonlinear vibrations of systems with many degrees of freedom". *Advances in Applied Mechanics,* **242(9)**, pp. 155–242.

[6] Renson, L., Noël, J., Kerschen, G., and Newerla, A., 2012. "Nonlinear modal analysis of the SmallSat spacecraft". In the Proceedings of the European Conference on Spacecraft Structures, Materials and Environmental Testing.

[7] Worden, K., Hickey, D., Haroon, M., and Adams, D. E., 2009. "Nonlinear system identification of automotive dampers: A time and frequency-domain analysis". *Mechanical Systems and Signal Processing,* **23**, pp. 104–126.

[8] Huang, J. L., Su, R. K. L., Lee, Y. Y., and Chen, S. H., 2011. "Nonlinear vibration of a curved beam under uniform base harmonic excitation with quadratic and cubic nonlinearities". *Journal of Sound and Vibration,* **330**, pp. 5151–5164.

[9] Wagg, D. J., 2005. "Periodic sticking motion in a two-degree-of-freedom impact oscillator". *International Journal of Non-linear Mechanics,* **40**, pp. 1076–1087.